

Multiscale Thermal Characterization of Mechanically Loaded Ceramic Matrix Composite

Estimation of Thermal Diffusivity at Micro/Mesoscale

J. El Yagoubi · J. Lamon · J.-C. Batsale · J. Dhote ·
M. Le Flem

Received: 27 May 2013 / Accepted: 3 December 2014 / Published online: 16 January 2015
© Society for Experimental Mechanics 2015

Abstract Ceramic Matrix Composites (CMC) are very attractive for structural applications at high temperatures or under temperature gradients. For these reasons, the mechanical properties must be considered together with the thermophysical properties. The aim of this work is to demonstrate the thermal characterization capabilities of IR thermography in multiscale damage assessment for CMCs. A first device was developed for the thermo-mechanical characterization at the level of fiber bundle. The longitudinal effective thermal diffusivity was monitored in-situ using the Angström method during a tensile test. In a second device, we implemented flash methods for the estimation of longitudinal and transverse diffusivities during tensile tests of 2D woven SiC/SiC composites. The macroscopic results corroborate the microscopic ones, but they also give complementary indications about composite's behavior. Moreover, these methods offered the

possibility to map the distribution of transverse thermal diffusivity.

Keywords Thermal diffusivity · Ceramic matrix composite · Infrared thermography · Damage

Introduction

Ceramic matrix composites (CMC), and more recently the polymer based composites, are used in structural components exposed to high temperatures or thermal cycling. For instance, SiC/SiC composites are potential candidates for nuclear fuel cladding [1–5]. This structural element is one of the most important safety barrier. The selected material must, in particular, allow the transfer of the generated heat flux (from the nuclear reaction) to the cooling system. Therefore, the thermal behavior of mechanically loaded composites is of primary importance.

Ceramic Matrix Composites (CMCs) are multiscale and architected materials. The service conditions (mechanical and thermal loadings, vibrations, etc.) generate several crack networks. It is shown that cracking occurs sequentially at different scales. The appropriate scales must be defined with respect to the characteristic size of heterogeneities and the damage mechanisms [6]. In the light of the cracking modes reported in the literature [7–12], two length scales are relevant [11]:

First, the microscale is a necessary step to capture the presence of fibers, the intratow matrix and the micropores. In addition, the characteristic damage mechanisms at this scale are the multiple matrix cracking and the fiber/matrix debonding [9, 13, 14]. Then, the mesoscale exhibits additional structural features: waviness, stacking characteristics and macropores. At this scale, transverse cracking and

J. El Yagoubi (✉) · J.-C. Batsale
University Bordeaux, I2M, UMR 5295, 33400 Talence, France
e-mail: jalal.el-yagoubi@u-bordeaux.fr

J.-C. Batsale
e-mail: jc.batsale@i2m.u-bordeaux1.fr

J. Lamon · J. Dhote
Laboratoire des Composites Thermostructuraux, UMR 5801,
33600 Pessac, France

J. Lamon
e-mail: lamon@lmt.ens-cachan.fr

M. Le Flem
CEA, DEN, DMN, 91191 Gif sur Yvette, France

Present Address:

J. Lamon
LMT-Cachan ENS Cachan/CNRS/Paris 6 University, 94230 Cachan,
France



delamination [7, 11, 15, 16] are the relevant damage mechanisms.

Several analytical and numerical models have been developed to compute the thermal properties of CMCs both at the microscale [17–19] and at the mesoscale [20–23]. Yet, these need reliable experimental data to validate the simulation tools as well as to identify model parameters. Infrared thermography is a suitable technique to investigate the effect of damage on thermal properties at the appropriate scale. The adaptability offered by the recent infrared cameras allows to design, at each scale, an experimental setup capable of monitoring the evolution of thermal diffusivity. For each experimental situation, we have to consider the most appropriate model that describes the heat transfers. The determination of the thermal diffusivity is achieved after solving the inverse problem. For this purpose, several methods were reported in the literature. The original flash method, initially developed by Parker et al. [24], was then extended to various experimental conditions [25–28]. In addition, Mourand et al. [29] proposed a method for the estimation of diffusivity distribution maps. The flash method was also used to determine the in-plane thermal diffusivity with a non-homogeneous heat generation [30–32]. As an alternative, we can consider the method proposed by Angström [33] and further similar techniques [34–37] in periodic regime to assess the longitudinal diffusivity.

The local disturbances induced by the cracks are revealed by infrared imaging. Thermal contrasts are potentially used in non-destructive testing of composites to detect delamination cracks in laminates [38] and impact damages [39]. Only a few attempts were focused on the investigation of the quantitative evolution of damage using thermal measurements. Pioneering works in [40] on unidirectional composites (RBSN/SiC_f) and in [41] on laminated composites have clearly demonstrated the effect of interfacial cracks on the thermal diffusivity. In [42], authors used thermal measurements to estimate the overall thickness of the air layer resulting from the delamination. The experimental results given in [21, 32, 43, 44], for multidirectional reinforced composites, showed that the measurement of thermal diffusivity during mechanical testing can be used to monitor the progression of damage. Sheikh et al. [45] reported a decrease in the global transverse thermal diffusivity of several CMCs under mechanical loading.

The aim of this work is to demonstrate the thermal characterization capabilities of IR thermography for multiscale damage assessment of fiber reinforced ceramic matrix composites. For this purpose, we developed two setups, one for the level of fiber bundle and the second one for the woven composite. From this experimental study, we highlighted the key insights in the interpretation of thermography analysis. These data are also useful for designing SiC/SiC fuel cladding.

Material

Two suitable composite specimens were prepared.

Minicomposite Test Specimens

Minicomposite test specimens (Fig. 1(a)) were made of single yarns consisting of approximately 500 commercial silicon carbide fibers (Hi-Nicalon S). The Pyrocarbon (PyC) interphase of few tens of nanometres and the silicon carbide matrix were deposited via Chemical Vapor Infiltration (SiC CVI). The properties of the constitutive materials are given in Table 1.

Figure 1(b) shows the different phases and the porosity inherent to the CVI process of matrix deposition. The matrix thickness ranges from 2–3 μm at the core to 8–10 μm at the rim. The cross sections of minicomposites are elliptical with an average area of 0.14 mm². The average fraction of fiber ($V_f = 0.38$) was estimated by image analysis.

Woven Composite Test Specimens

The composite consists of 11 plies of plain fabrics (Fig. 1(b)) manufactured via Chemical Vapor Infiltration (SAFRAN Group). A layer of pyrocarbon interphase (100 nm thick) and the SiC matrix were deposited on the fiber preform (Hi-Nicalon S). The final composite plate was 3 mm thick.

The fractions of fiber, matrix and porosity were determined using image analysis. The results are summarized in Table 2. In addition, it was found that the average number of fibers is approximately 500 per bundle, and that the average filament diameter is 12.7 μm (±2.7).

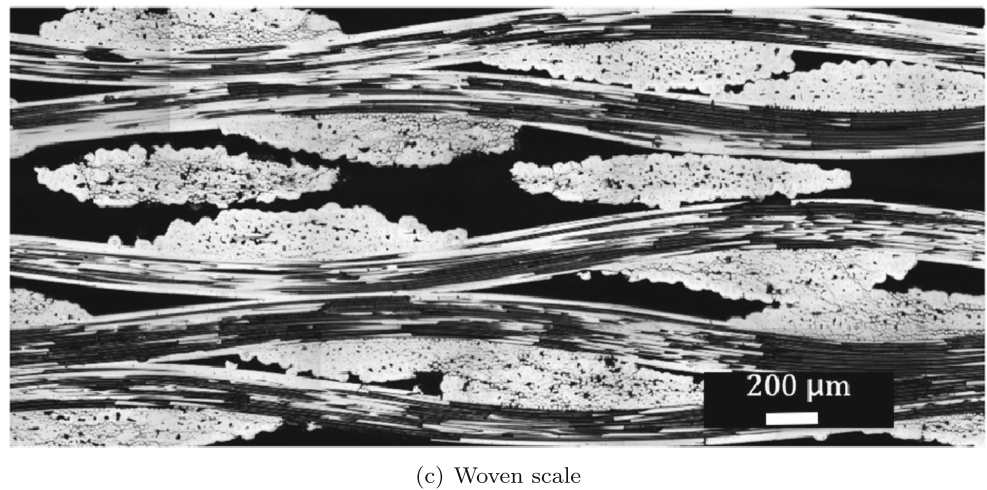
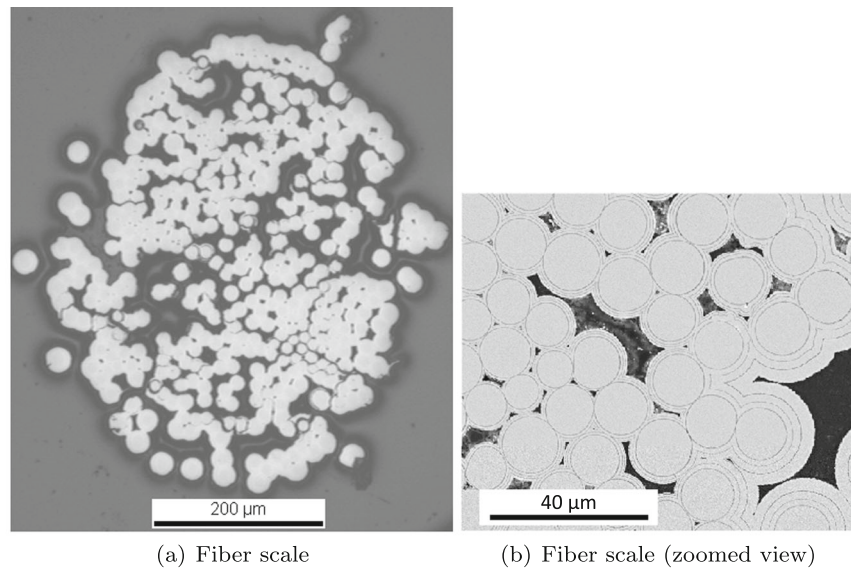
Moreover, the overall fraction of porosity was estimated to be 30 % by means of several porosimetry techniques (water, ethanol, mercury, and helium-based picnometry). It should be noted that this is quite high. Authors in [7, 9, 16, 50] reported volume fractions of porosity in the range of 10 to 15 % for similar composites.

Table 1 Selected properties of SiC fibers and SiC matrix (at 25 °C) from ^a [46], ^b [47], ^c [48] and ^d [49]

	Hi-Ni-S	SiC matrix
Diameter (μm)	13 ^a	–
Young's modulus (GPa)	408 ^a	400 ^d
Strain to failure (%)	0.63 ^a	–
Density (g.cm ⁻³)	3 ^a	2.74 ^a
Thermal conductivity (W.m ⁻¹ .K ⁻¹)	18 ^b	67 ^b
Specific heat capacity (J.kg ⁻¹ .K ⁻¹)	700 ^c	690 ^c
Thermal diffusivity (mm ² .s ⁻¹)	8.6	4.4



Fig. 1 Micrographs of the Ceramic Matrix Composite materials (SiC/SiC) under investigation



Experimental

Two experimental setups (Fig. 2) were developed in order to investigate simultaneously the thermal and the mechanical behaviors of minicomposite and composite specimens. In the following, both experimental setups are described in detail.

Table 2 Volume fractions of the constituents of the woven ceramic matrix composite (SiC/PyC/SiC) under study

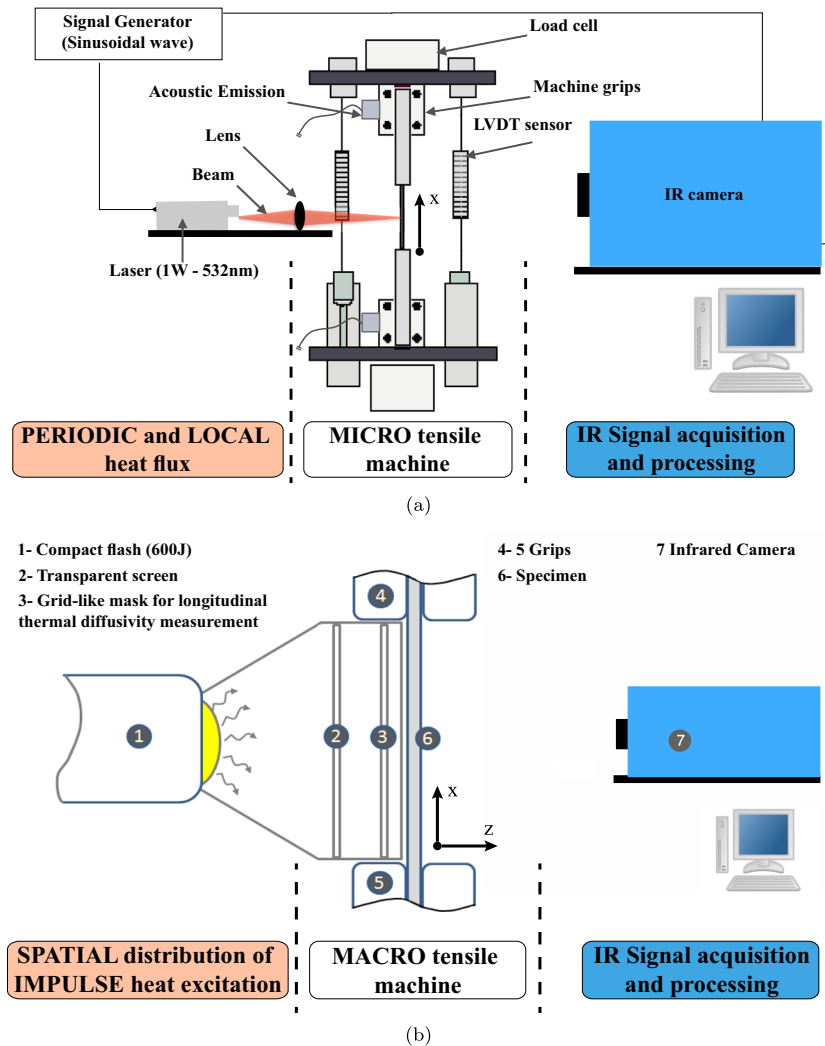
	Microporosity	Fiber	Matrice	Mesoporosity
Intratow	0.03	0.42	0.55	–
Global	0.02	0.29	0.39	0.3

Tensile Tests

On minicomposite specimens

Tensile tests were performed using an electromechanical testing machine (MTS). Metallic cylindrical tabs were attached at specimen's ends. The spacing distance (gage length) was 30 mm. Specimen strains were measured using two inductive sensors (LVDT). Tensile tests were carried out under quasi-static conditions with a crosshead displacement rate of 0.05 mm/min. Testing procedure also included loading-unloading loops to monitor the decrease in the elastic modulus. The crosshead was kept immobile during thermal measurements. It is worth noting that the testing machine was also equipped with two acoustic emission sensors to check that damage did not progress in the time period during which thermal diffusivity measurement was performed.

Fig. 2 Experimental setups for the mechanical and thermal characterization of the composites under uniaxial tensile test: (a) minicomposite and (b) woven composite test specimens



On composite specimens

An electromechanical tensile machine with hydraulic grips (Instron 4505) was used. Metallic tabs (length=25 mm, width=19 mm) were affixed to the ends of $118 \times 19 \times 3 \text{ mm}^3$ specimens. Quasi-static conditions with a displacement speed of 0.05 mm/min were applied. The deformations of composite were measured using two mechanical extensometers placed on both sides of the sample. The gage length was 25 mm. Again, testing procedure also included loading-unloading loops to monitor the decrease in the elastic modulus. Acoustic emission sensors revealed that the damage did not progress in the time period during which thermal diffusivity measurement was performed.

Thermal Diffusivity Measurements

Principle

Unsteady thermal conditions are appropriate for the estimation of the thermal diffusivity from temperature evolution.

The heat source have to be applied in order to maximize the heat transfers during the thermal measurement. For this purpose, the specimen geometry, the material thermal properties and the equipment characteristics (spatial resolution, acquisition frequency, etc.) must be taken into account. An interesting approach consists in the evaluation of the characteristic times based on the Fourier number (Fo , (1)):

$$Fo = \frac{a_c \cdot t_c}{d_c^2} \quad (1)$$

When $Fo = 1$, t_c is the time period during which heat passes through a medium of thickness d_c and thermal diffusivity a_c . It indicates the time period for measurement of the transient thermal properties, which has to be consistent with the acquisition frequency of the infrared signal. The magnitudes of the characteristic times (t_c) associated to the heat transfer in the different directions are given in Table 3.

Table 3 Magnitude of characteristic times (t_c) associated to the heat transfers in the directions parallel (\parallel) and perpendicular (\perp) to the fiber reinforcement (d_c and a_c are the corresponding length and thermal diffusivities)

	\parallel	\perp (minicomposite)	\perp (composite)
d_c	1 cm	100 μm	3 mm
a_c	10 mm^2s^{-1}	1 mm^2s^{-1}	1 mm^2s^{-1}
t_c	10s	1μs	1s

First, only small temperature differences can be expected across the minicomposite's section ($\sim 100\mu\text{m}$), even in the case of strong gradients, and this would lead to a poor signal/noise ratio. Nevertheless, at this small length scale, periodic steady state is reached rapidly and the Angström [33] method is suitable.

Then, at larger length scales (woven composite) the periodic methods become less pertinent. For composite plates, the flash methods are well-suited because the transverse and the in-plane diffusivities can be simultaneously estimated [32]. In addition, the maps of transverse thermal diffusivity can also be obtained.

Application to the minicomposite test specimens

The selected method was initially proposed by Angström [33] and then adapted by several authors [34–37]. It consists in creating a local oscillating heat source and then processing the temperature profile along the axial direction. When the periodic steady state is reached, a damped out of phase thermal wave propagates through the solid medium. The estimation procedure of the longitudinal thermal diffusivity, which is detailed in Appendix A.1, is based on the evaluation of the damping and phase shifts.

The local modulated heat source is provided by a laser beam of 532 nm wavelength emitted by a diode (1 Watt). The laser beam is powered by a signal generator that produces sine waves at the selected frequency. Then, the laser beam passes through a lens to be focused on a diameter of about 100 μm at the specimen's surface. The thermal excitation system (diode and lens) is mounted on a three axes precision positioning stage to control the position of the spot. Thus, the heat source is generated at the center of the minicomposite specimen mounted in the grips of the tensile machine.

An infrared camera (Titanium 520 M from FLIR) captures the infrared signal (IR) emitted by the outer surface of the specimen. It has 320x256 InSb sensors and it is equipped with a 50 mm objective with an extension ring to reduce the spatial resolution to a size of about 80 μm . The infrared images are recorded at 100 Hz. Then a dedicated software (Altair-LI also supplied by FLIR) is used to compute the maps of damping and phase shift. The reference

phase is assumed to be given by the signal generator that is connected to the appropriate Lockin input of the camera. Finally, at each loading step, the apparent in-plane thermal diffusivity is estimated according to the procedure described in Appendix A.1.

Application to composite test specimens

We developed a setup capable of monitoring both in-plane (a_x^w) and transverse (a_z^w) diffusivities. This was achieved by implementing two variants of the Flash method. The front face of composite samples was heated using a flash lamp (600J) while the thermal response was recorded at the rear face using the same Infrared camera as in the first setup. Either homogeneous (transverse diffusivity [29]) or spatially periodic (longitudinal diffusivity [30]) heat irradiation was generated. A transparent film was placed between the flash lamp and the specimen as a barrier against the convective heat transfer. Then, a grid-like mask with periodic openings was added for the estimation of the global in-plane diffusivity (a_x^w). A randomly distributed heat can be alternatively used [31], particularly to get maps of in-plane diffusivity. The interest of the periodic pattern lies essentially in the fact that a unique frequency is emphasized.

The grid period was chosen depending on the specimen thickness, the transverse and the in-plane diffusivities [32]. The optimal period may not be constant during the test because of the damage progress.

We performed the diffusivity measurements under constant load: at each load step two experiments were performed for the determination of a_z^w and three for a_x^w . The recording frequency of the infrared camera was 150 Hz and the spatial resolution was about 250 μm . The infrared signals were then processed as described in Appendix A.2.

Multiscale Analysis of Damage

In this section, we examine in detail the thermal and the mechanical results to end up with an original interpretation of the processed infrared data. Since the mechanical behavior of the materials under study is documented enough, the mechanical tests were used to infer meaningful data about the damage *scenarii*. On this basis, we propose to assess the sensitivity of the IR thermography to the various well-known damage modes.

Elastic Damageable Behavior

Under thermomechanical loadings, the Ceramic Matrix Composites display an elastic damageable behavior. The physical mechanisms responsible for the nonlinearity in the mechanical behavior are cracks that form in the matrix or



at the fiber/matrix interphase. The damage scenario may depend on the texture, the loading mode, the nature of fiber, the interphase and the matrix.

For both the minicomposite and the woven composite specimens, the tensile stress-strain curves (Fig. 3) exhibit the features of the well-known elastic damageable behavior of CMCs [8, 9, 13, 50–52]. The examination of the tensile tests revealed several relevant observations:

- The stress-strain curves show different stages that can be associated to the sequenced damage process. The first stage is the linear elastic domain of deformations for strains smaller than 0.1 %. The linear domain ended at slightly smaller strains for the woven composite specimens because of the size effects. Then, a non linear domain with upward curvature is indicative of increasing compliance associated to the transverse matrix cracking (for strains smaller than 0.35 %). A second linear domain, indicative of constant compliance, is attributed to the deformation of fibers. For strains close to the ultimate failure, a non linear domain with upward curvature is indicative of fiber failures.
- Also, the loading-unloading cycles demonstrate a decrease in the material stiffness. It is worthy noting that the ratio of elastic modulus to initial modulus is a classical damage indicator.
- The loading-unloading cycles also highlight the presence of residual strains and hysteresis loops. These are both indicative of dissipative mechanisms such as cracking and friction at fiber/matrix interfaces.

Key Insights in the Interpretation of Thermography

As cracks form, part of the energy provided to the composite material is dissipated:

- in the creation of new surfaces
- in fiber/matrix friction (heat sources).

In theory, both dissipation modes could be detected using infrared thermography. The creation of new surfaces results in a thin insulating layer (contact resistance and air) which subsequently reduces the thermal diffusivity. The friction phenomena could lead to an increase in temperature. In the following, we evaluate the sensitivity of the thermal diffusivity to the different cracking modes. In addition, we highlight the main useful information inferred from the thermography analysis.

In-plane thermal diffusivity

Figure 4(a) depicts the evolution of the normalized thermal diffusivity for the minicomposite and the woven composite specimens during a tensile test. In both cases, the global

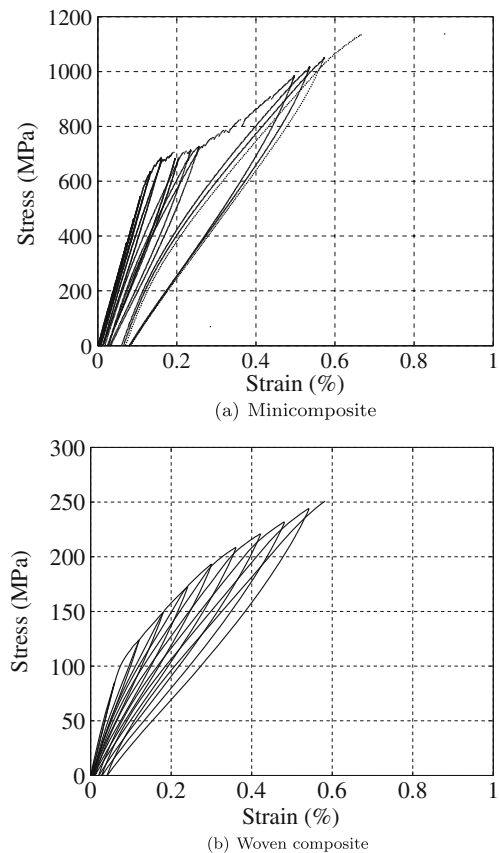
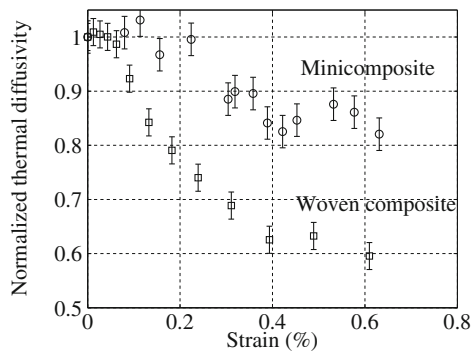


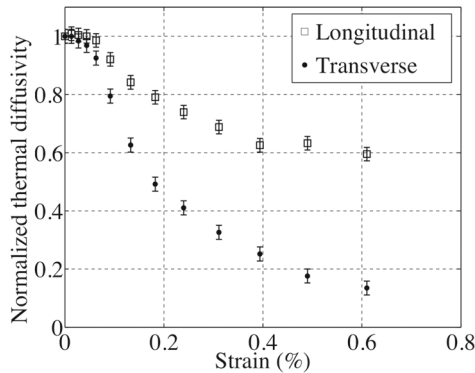
Fig. 3 Tensile stress-strain curves for the minicomposite and the woven composite specimens

longitudinal thermal diffusivity decreases with increasing applied strain. Interestingly, the minicomposite and the woven composite display a similar behavior.

- The thermal diffusivity remained constant during the linear elastic domain.
- Then, the diffusivity experienced a drop in the deformation domain ranging from the end of the elastic domain to about 0.35 %. For the minicomposite, a single mode of matrix cracking was observed. It consists of cracks perpendicular to the loading direction and distributed along the fiber axis. For the woven composite, several cracking modes were reported in the literature and observed using post-mortem microscopy. In addition to the cracks in longitudinal tows, which are equivalent to matrix cracks in minicomposites, the woven composites develop two types of transverse cracks in the transverse tows [23]: Type-1 cracks perpendicular to loading direction while type-2 cracks are in-the-plane. Weaviness and the presence of various transverse cracks can explain that the composite diffusivity was more affected than the minicomposite's one.
- After matrix cracking saturation, the thermal diffusivity remained barely constant until the ultimate fracture.



(a) Longitudinal thermal diffusivity for minicomposite and woven composite specimens



(b) Longitudinal and transverse diffusivity for woven composite specimens

Fig. 4 Evolution of the global thermal diffusivity of the minicomposite and the woven composite (normalized using the diffusivity of the undamaged material $\frac{a}{a_0}$) measured during a tensile test

In this regime, the predominant phenomena are the sliding at fiber/matrix interfaces and the interlaminar debonding for the woven composite. The experimental results show that the in-plane thermal diffusivity was

not affected by these damage modes because, in this case, crack lips were parallel to the heat flux.

- The fiber breakage is the stochastic degradation mechanism responsible for the ultimate fracture of the minicomposite and the composite specimens. It was not possible to capture the effect of the fiber ruptures on the thermal diffusivity since it is an unstable phenomenon. Nevertheless, the thermographic images at failure show that the heat sources were only generated within the longitudinal tows (loading direction). This observation confirms that the final failure of composite results from the breakage of fiber tows.

Transverse thermal diffusivity

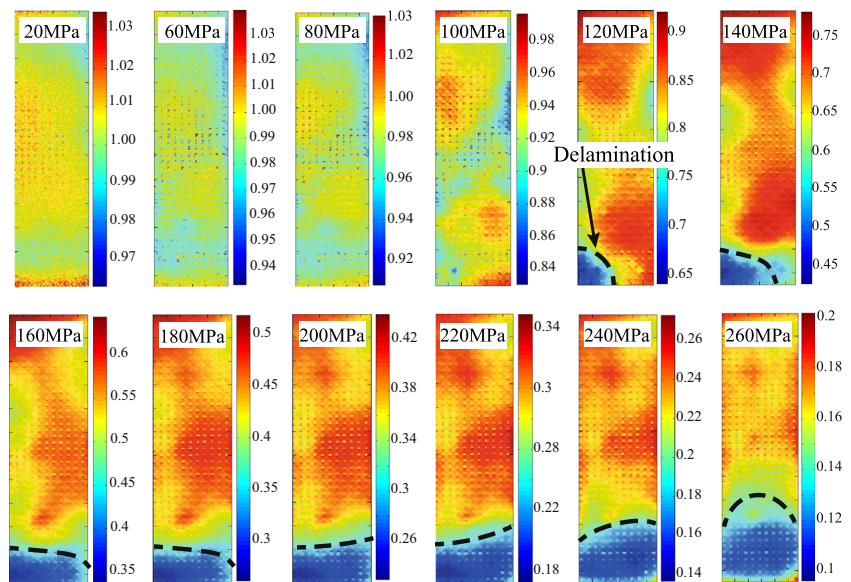
Interestingly, the characterization of the transverse thermal diffusivity allowed us to investigate damage from both global and local viewpoints.

Figure 4(b) depicts the decrease in the global in-plane and transverse thermal diffusivities of the woven composite specimens during a tensile test. Yet, two main differences need to be discussed.

First, the experimental data demonstrate that the transverse thermal diffusivity was significantly more affected than the longitudinal one. Figure 4(b) shows that a_z^w experienced a steeper drop and 80 % decrease at the end of the test, against 40 % for a_x^w . The experimental results provide interesting observations regarding the spatial distribution of the transverse thermal diffusivity: Fig. 5 depicts the local variation of a_z^w . In particular, the maps highlight that the transverse damage is highly heterogeneous for applied stresses higher than 100 MPa.

In addition, it appears that the transverse thermal diffusivity kept decreasing even for strains higher than 0.4 %

Fig. 5 Evolution of the transverse thermal diffusivity maps during tensile test: Illustration of the initiation and the propagation of the delamination in woven SiC/SiC composite specimens



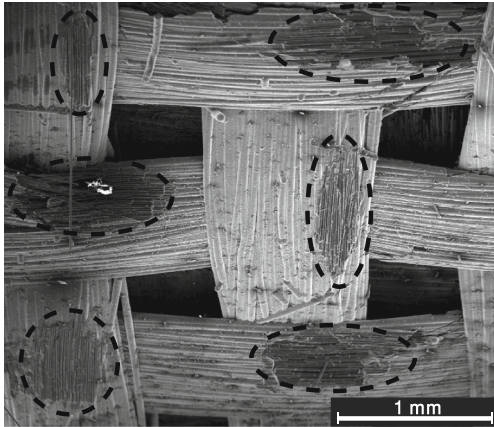


Fig. 6 Scanning electron microscopy images of the interply delamination

while the longitudinal one remained barely constant in the same deformation range. This confirms that, in this regime, the preponderant phenomena are related to interfacial degradation (interlaminar and interlaminar interfaces) and sliding. In fact, Fig. 5 clearly evidences the initiation of a delamination crack which propagates in a parallel direction to the load until the ultimate rupture. Furthermore, the micrograph in Fig. 6 shows evidences of delamination. This highlights the size of the contact area between plies. It is worth noting that these interfacial damage modes do affect the transverse diffusivity whereas the in-plane one was not sensitive to these mechanisms.

From a global point of view, the experimental results can be discussed with respect to the composite architecture. In particular, it appears that the initial material anisotropy contributes to further damage-induced anisotropy in the thermal behavior.

Conclusion

The thermal properties of ceramic matrix composite under mechanical loading were successfully investigated. The conclusions from this study are as follows:

- This work is demonstrative of the capability of Infrared Thermography for the study of damage progress at various pertinent length scales.
- It was shown that the use of thermography can provide a better understanding of the damage mechanisms. This approach is also able to capture anisotropic and highly heterogeneous evolution of damage, which can be related to the composite architecture (fiber's orientation).
- The experimental data confirmed that the minicomposite test specimens represent a relevant intermediate level

to study the damage of CMCs and particularly to predict the composite ultimate failure.

- The flash methods were found to be the most promising techniques. The thermal diffusivities (maps) as a function of load can be used as inputs in the quantitative analysis of the generated heat sources. Also, the diffusivity-damage relationships, identified in this work, can serve as tools for the monitoring of structures under in-service conditions.

Acknowledgments This work has been supported by C.N.R.S. and CEA through a grant given to J. E.. The authors are grateful to B. Humez for the support in the mechanical test.

Appendix A: Infrared Signal Processing

A.1 Lock-In Thermography

Angström [33] measured the thermal diffusivity of a long and homogeneous isotropic metallic bar. A periodic heat flux was generated and the temperature was measured at the specimen surface. Assuming one-dimensional heat transfer, this experiment can be described by the partial differential equation in equation (2) with the boundary and initial conditions given in equation (3):

$$\frac{\partial^2 T}{\partial x^2} - \frac{hp}{\lambda_x S} T = \frac{1}{a_x} \frac{\partial T}{\partial t} \quad (2)$$

Where h is the convective heat transfer coefficient, p is the perimeter, S is the cross-sectional area, λ_x and a_x are respectively the longitudinal thermal conductivity and the diffusivity.

$$\begin{aligned} t = 0 & \quad T(x, t) = 0 \\ x = 0 & \quad -\lambda_x \frac{\partial T}{\partial x} = \phi_o + \Delta\phi_o \sin(\omega t + \varphi_o) \\ x \rightarrow \infty & \quad T(x, t) = 0 \end{aligned} \quad (3)$$

The local heat flux is described by the following quantities: ϕ_o is the offset, $\Delta\phi_o$ is the amplitude, ω is the pulsation and φ_o is the reference phase. For the purpose of thermal diffusivity identification, the focus is only on the periodic components ($T^*(x, t)$) given in equation (4):

$$T^*(x, t) = A(x) \cos(\omega t + \varphi(x)) \quad (4)$$

The amplitude and the phase difference of the wave are respectively given by equations (5) and (6):

$$A(x) = A_o \exp(-z_r x) \quad (5)$$

$$\varphi(x) = \varphi_o - z_i x \quad (6)$$

where the product of terms (z_i, z_r) is denoted z_π (equation (7)):

$$z_\pi = z_i \cdot z_r = \frac{\omega}{2a_x} \tag{7}$$

Then, for several experiments conducted at different pulsations (k experiments), the previous scalar (equation (7)) turns to a vectorial expression (equation (8)):

$$\underline{Z}_\pi = \frac{1}{2a_x} \underline{\Omega} \tag{8}$$

where $\underline{\Omega}$ and \underline{Z}_π are the vectors associated to ω and z_π . Finally, the longitudinal thermal diffusivity is calculated using the least squares method [37]:

$$a_x = \frac{1}{2(\underline{\Omega}^T \cdot \underline{\Omega})^{-1} \cdot \underline{\Omega}^T \cdot \underline{Z}_\pi} \tag{9}$$

A.2 Flash Methods

The following paragraphs describe the methods implemented for the estimation of the transverse thermal diffusivity maps and the global in-plane thermal diffusivity.

Transverse thermal diffusivity

This work proposes first to consider simple estimation methods for the transverse diffusivity mapping. Such methods consist in validating the implementation of 1D heat transfer models through the thickness, in the case of uniform flash irradiation. Assuming unidirectional heat transfers, the temperature evolution, at a given position of the rear face $(x,y,z=e)$, is a function of the local transverse thermal diffusivity $a_z(x,y)$ and other parameters (the heat capacity C_p , the density ρ , the energy density $Q(x,y)$, etc.). In the ideal case, the sample (thin plane plate) is assumed to be thermally insulated and with an initially uniform temperature field. Then, the temperature response to a thermal pulse, at a location (x,y) equivalent to a pixel, is given below (equation (10)):

$$T^{1D}(x, y, z = e, t) = \frac{Q(x, y)}{\rho C_p e} \times f(t, a_z^w(x, y)) \tag{10}$$

where $f(t, a_z^w)$ is as follows:

$$f(t, a_z^w) = 1 + 2 \sum_{n=1}^{n=\infty} \cos(n\pi) \exp\left(\frac{-n^2 \pi^2 a_z^w t}{e^2}\right) \tag{11}$$

Figure 7 depicts the evolution of the average temperature at the rear face of the woven composite specimen under tensile test for increasing applied stresses (0 MPa to 240 MPa). In the reference [29], the authors proposed to estimate the local

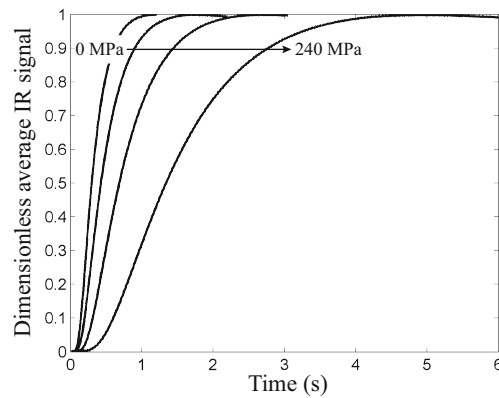


Fig. 7 Evolution of the average temperature at the rear face of the woven composite specimen under tensile test: from the left to the right 0 MPa, 140 MPa, 180 MPa et 240 MPa

thermal diffusivities using a first order asymptotic expansion (equation (12)) for diffusivities close to the average transverse diffusivity denoted a_{z0}^w :

$$T(x, y, t) \simeq T^{1D}(z = e, t, a_{z0}) + (a_z^w(x, y) - a_{z0}^w) \frac{\partial T^{1D}}{\partial a_z^w} \Big|_{a_{z0}^w} \tag{12}$$

Equation (12) can be written as a linear system of equations as given in equations (13) and (14). This linear system is solved at each pixel (x, y) .

$$T(x, y, t) \simeq \left[f(t, a_{z0}^w) \frac{\partial f}{\partial a_z^w} \Big|_{a_{z0}^w} \right] \cdot \left[\frac{Q}{\rho C_p e} \cdot (a_z^w(x, y) - a_{z0}^w) \right] \tag{13}$$

$$Y^z(x, y) = X^z(x, y) \cdot \beta^z(x, y) \tag{14}$$

The matrix $\beta^z(x, y)$ is then estimated using the least squares method (equation (15)).

$$\beta^z(x, y) = \left((X^z(x, y))^T X^z(x, y) \right)^{-1} (X^z(x, y))^T Y^z(x, y) \tag{15}$$

The local transverse thermal diffusivity is finally estimated according to equation (16):

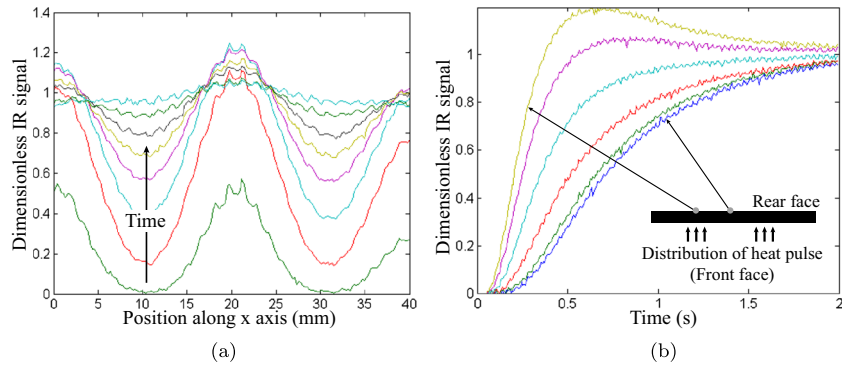
$$a_z^w(x, y) = a_{z0}^w + \frac{\beta^z(2)_{(x,y)}}{\beta^z(1)_{(x,y)}} \tag{16}$$

In-plane thermal diffusivity

In order to estimate the global in-plane diffusivity, a second flash method with non-uniform irradiation was implemented. The front face of the composite was irradiated at spatially periodic bands. The resulting spatial distribution



Fig. 8 (a) Profiles of temperature (along x axis) and (b) thermograms at the rear face of a woven composite specimen during a flash experiment performed with a grid-like mask



and the evolution of the infrared signal collected at the rear face are depicted in Fig. 8. Philipi et al. [30] proposed a robust method to estimate the global in-plane thermal diffusivity. It is based on the assumption that the in-plane and the transverse heat transfers are uncorrelated. It is worth noting that this assumption is not necessarily valid for multilayered composite material with elementary layers made of different materials (or different orientations). However, Maillet et al. [53] showed that the assumption holds for the material under study, which was made of identical layers with contact resistances. Then, in the Fourier-Laplace space, the rear face temperature can be written as follows equation (17):

$$\Theta(\alpha_n, z = e, p) = \int_0^L \int_0^\infty \frac{T(x, z = e, t)}{\cos(\alpha_n x) \cdot \exp(-pt)} dt dx \quad (17)$$

where L is the length of the composite along the x axis, and α_n is defined as follows:

$$\alpha_n = \frac{n\pi}{L} \quad (18)$$

where n is an integer.

It is shown in [30] that the solution of equation (17) can be written as follows (equation (19)):

$$\Theta(\alpha_n, z = e, p) = \mathcal{H}\left(p + a_x^w \alpha_n^2\right) \quad (19)$$

with

$$\mathcal{H}(p) = \Theta(\alpha_n = 0, z = e, p) \quad (20)$$

With $\mathcal{T}(\alpha_n, z = e, t)$ being the fourier transform of $T(x, z = e, t)$, the inverse Laplace transform of equation (19) is then given in equation (21):

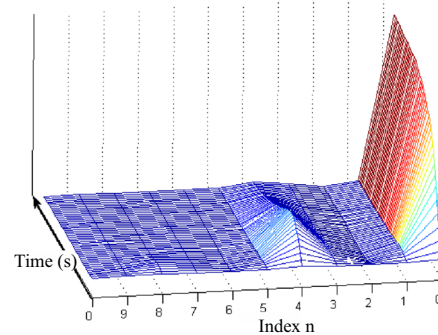
$$\mathcal{T}(\alpha_n, z = e, t) = \mathcal{T}(\alpha_n = 0, z = e, t) \cdot \exp\left(-a_x^w \alpha_n^2 t\right) \quad (21)$$

Fourier transform of the temperature field obtained during a flash experiment is plotted in Fig. 9(a). Then, the in-plane thermal diffusivity a_x^w can be estimated by solving the following linear relation given in equation (22):

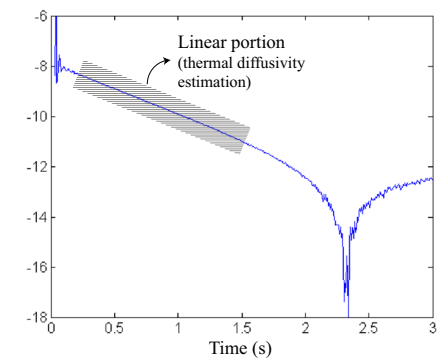
$$\ln\left(\frac{\mathcal{T}(\alpha_n, z = e, t)}{\mathcal{T}(\alpha_n = 0, z = e, t)}\right) = -a_x^w \alpha_n^2 t \quad (22)$$

which can be put in the classical form as follows (equation (23)):

$$Y^x(t) = X^x(t) \beta^x \quad (23)$$



(a) Fourier transform of the IR signal



(b) $\ln\left(\frac{\mathcal{T}(\alpha_n, z = e, t)}{\mathcal{T}(\alpha_n = 0, z = e, t)}\right)$ calculated for $n=4$. The global in-plane thermal diffusivity is estimated from the linear portion of this curve.

Fig. 9 Analysis of the fourier transform of the IR signal measured at the rear face of the woven composite specimen



where Y^x is derived from the infrared signal, X^x is equal to $-\alpha_n^2 t$ (for $n=4$), and β^x is the parameter to identify.

$$\beta^x = a_x^w = \left(X^x(t) \right)^T X^x(t) \right)^{-1} \left(X^x(t) \right)^T Y^x(t) \quad (24)$$

Figure 9(b) depicts the evolution of Y^x . The global in-plane thermal diffusivity (a_x^w) was calculated according to equation (24) in the time window when Y^x decreased linearly.

References

- Jones RH, Steiner D, Heinisch HL, Newsome GA, Kerch HM (1997) Radiation resistant ceramic matrix composites. *J Nucl Mater* 245:87–107
- Youngblood GE, Senor DJ, Jones RH, Graham S (2002) The transverse thermal conductivity of 2d-sic/sic composites. *Comp Sci Tech* 62:1127–1139
- Zinkle SJ, Busby JT (2009) Structural materials for fission and fusion energy. *Mater Today* 12:12–19
- Yvon P, Carré F (2009) Structural materials challenges for advanced reactor systems. *J Nucl Mater* 385:217–222
- Hallstadius L, Johnson S, Lahoda E (2012) Cladding for high performance fuel. *Progress Nucl Ener* 57:71–76
- Michel J-C, Moulinec H, Suquet P (2001) Composites à microstructure périodique. In: Bornert M, Bretheau T, Gilormini P (eds) *Homogénéisation en mécanique de matériaux 1: Matériaux aléatoires élastiques et milieux périodiques*. Hermès, pp 95–132
- Aubard X, Lamon J, Allix O (1994) Model of the nonlinear mechanical behavior of 2d sic-sic chemical vapor infiltration composites. *J Am Ceram Soc* 77:2118–2126
- Guillaumat L, Lamon J (1996) Probabilistic-statistical simulation of the non-linear mechanical behavior of a woven sic/sic composite. *Comp Sci Tech* 56:803–808
- Guillaumat L, Lamon J (1996) Fracture statistics applied to modelling the non-linear stress-strain behavior in microcomposites: influence of interfacial parameters. *Int J Fract* 82:297–316
- Lamon J, Thommeret B, Percevault C (1998) Probabilistic-statistical approach to the matrix damage and stress-strain behavior of 2d woven sic/sic ceramic matrix composites. *J Eur Ceram Soc* 18:1797–1808
- Lamon J (2002) Micromechanics-based approach to the mechanical behavior of brittle matrix composites. *Comp Sci Tech* 61:2259–2272
- Pailler F, Lamon J (2005) Micromechanics based model of fatigue/oxidation for ceramic matrix composites. *Comp Sci Tech* 65:369–374
- Lissart N, Lamon J (1997) Damage and failure in ceramic matrix minicomposites: experimental study and model. *Acta Mater* 45:1025–1044
- Naslain R, Lamon J, Pailler R, Bourrat X, Guette A, Langlais F (1999) Micro/minicomposites: a useful approach to the design and development of non-oxyde cmcs. *Comp Part A* 30:537
- Carrère P, Lamon J (2003) Creep behaviour of a sic/si-b-c composite with a self-healing multilayered matrix. *J Eur Ceram Soc* 23:1105–1114
- Forio P, Lavaire F, Lamon J (2004) Delayed failure at intermediate temperatures (600c-700c) in air in silicon carbide multifilament tows. *J Am Ceram Soc* 87:888–893
- Hasselmann DPH, Johnson LF (1989) Effective thermal conductivity of composites with interfacial thermal barrier resistance. *J Comp Mater* 21:508–514
- Lu TJ, Hutchinson JW (1995) Effect of matrix cracking on the overall thermal conductivity of fibre-reinforced composites. *J Phil Trans Roy Soc* 351:595
- Tang C, Blacklock M, Hayhurst DR (2009) Uni-axial stress-strain response and thermal conductivity degradation of ceramic matrix composite fibre tows. *Proc R Soc A* 465:2849–2876
- Del Puglia P, Sheikh MA, Hayhurst DR (2004) Modelling the degradation of thermal transport in a cmc material due to three different classes of porosity. *Modelling Simul Mater Sci Eng* 12:357–372
- Farooki JK, Sheikh MA (2006) Finite element modelling of thermal transport in ceramic matrix composites. *Comp Mater Sci* 37:361–373
- Tang C, Blacklock M, Hayhurst DR (2011) Stress-strain response and thermal conductivity degradation of ceramic matrix composite fiber tows in 0-90° uni-directional and woven composites. *J Comp Mat* 45:1461–1482
- El Yagoubi J (2011) Effect of damage on thermal properties of ceramic matrix composites: a multiscale approach. Phd thesis, University of Bordeaux
- Parker WJ, Jenkins RJ, et Butler CP, Abbott GL (1961) Flash method of determining thermal diffusivity, heat capacity, and thermal conductivity. *J Appl Phys* 32:1679–1684
- Cowan RD (1963) Pulse method of measuring thermal diffusivity at high temperatures. *J Appl Phys* 34:926–927
- Cape JA, Lehman GW (1963) Temperature and finite pulse-time effects in the flash method for measuring thermal diffusivity. *J Appl Phys* 34:1909–1913
- Larson KB, Koyama K (1967) Correction for finite-pulse-time effects in very thin samples using the flash method of measuring thermal diffusivity. *J Appl Phys* 38:465–474
- Taylor RE, Clark LM (1974) Finite pulse time effect in flash diffusivity method. *High Temp-High Press* 6:65–72
- Mourand D, Gounot J, Batsale JC (1998) New sequential method to process noisy temperature response from flash experiment measured by infrared camera. *Rev Sci Instrum* 69:1437–1440
- Philippi I, Batsale JC, Maillat D, Degiovanni A (1994) Measurement of thermal diffusivity through processing of infrared images. *Rev Sci Instrum* 66:182–192
- Batsale JC, Battaglia JL, Fudym O (2004) Autoregressive algorithms and spatially random flash excitation for 2d non destructive evaluation with infrared cameras. *QIRT J* 1:5–20
- Krapez JC, Spagnolo L, Frieb M, Maier HP, Netter F (2004) Measurement of in-plane diffusivity in non homogeneous slabs by applying flash thermography. *Int J Thermal Sci* 43:967–977
- Angström AJ (1861) Bestimmung der warme leitung durch periodische temperaturänderung. *Annalen der Physikund Chemie* 114:513–530
- King RW (1915) A method of measuring heat conductivities. *Phys Rev* 6:437–445
- Preston T (1929) *Theory of heat*, 4th edn. Macmillan Company, London, p 627
- Starr C (1937) An improved method for the determination of thermal diffusivities. *Rev Sci Instrum* 8:61–64
- Pradère C, Goyhénèche JM, Batsale JC, Dilhaire S, Pailler R (2006) Thermal diffusivity measurements on a single fiber with microscale diameter at very high temperature. *Int J Therm Sci* 45:443–451
- Balageas DL, Déom AA, Boscher DM (1987) Characterization and nondestructive testing of carbon-epoxy composites by a pulsed photothermal method. *Mater Eval* 45:456–465



39. Bhatt RT, Choi SR, Cosgriff LM, Fox DS, Lee KN (2008) Impact resistance of environmental barrier coated sic/sic composites. *Mater Sci Eng A* 476:8–19
40. Bhatt H, Donaldson KY, Hasselman DPH, Bhatt RT (1990) Role of the interfacial thermal barrier in the effective thermal diffusivity/conductivity of sic-fiber-reinforced reactionbonded silicon nitride. *J Am Ceram Soc* 73:312–316
41. Hasselman DPH, Venkateswaran A, Tawil H (1991) Role of interfacial debonding and matrix cracking in the effective thermal diffusivity of sic-fibre-reinforced chemical vapour deposited sic matrix composites. *J Mater Sci Lett* 10:1037–1042
42. Guillaumat L, Batsale JC, Mourand D (2004) Real time infrared image processing for the detection of delamination in composite plates. *Compos Part A* 35:939–944
43. Bamford M, Batsale JC, Fudym O (2009) Nodal and modal strategies for longitudinal thermal diffusivity profile estimation: application to the non destructive evaluation of sic/sic composites under uniaxial tensile tests. *Infrared Phys Technol* 52:1–13
44. Bamford M, Florian M, Vignoles GL, Batsale JC, Cairo CAA, Maillé L (2009) Global and local characterization of the thermal diffusivities of sic/sic composites with infrared thermography and infrared ash method. *Comp Sci Tech* 69:1131–1141
45. Sheikh MA, Hayhurst DR, Taylor SC, Taylor R (2009) Experimental investigation of the effect of mechanical loading on thermal transport in ceramic matrix composites. *J Multiscale Modelling* 1:403
46. Dong SM, Chollon G, Labrugère C, Lahaye M, Guette A, Bruneel JL, Couzi M, Naslain R, Jiang DL (2001) Characterization of nearly stoichiometric sic ceramic fibers. *J Mat Sci* 36:2371–2381
47. Yamada R, Igawa N, Taguchi T, Jitsukawa S (2002) Highly thermal conductive, sintered sic fiber-reinforced 3d-sic/sic composites: experiments and finite-element analysis of the thermal diffusivity/conductivity. *J Nucl Mater* 307:1215–1220
48. Sauder C (2004) Effect of irradiation on SIC fibres. Internal report, LCTS
49. Lamon J, Lissart N, Rechigniac C, Roach DM, Jouin JM (1993) Micromechanical and statistical approach to the behavior of cmc's. In: *Composites and advanced ceramics - Proceedings of the 17th annual conference and exposition - ceramic engineering and science proceedings*. Cocoa Beach (Florida) - USA
50. Carrère P (1996) Comportement thermomécanique d'un composite de type SiC/SiC. Phd thesis, University of Bordeaux
51. Aubard X (1992) Modélisation et identification du comportement mécanique des matériaux composites 2d SiC/SiC. Phd thesis, University of Bordeaux
52. Forio P (2000) Thermomechanical behavior and lifetime of a SiC/SiC composite with a self healing matrix. Phd thesis, University of Bordeaux
53. Maillet D, André S, Batsale JC, Degiovanni A, Moyne C (2000) *Thermal quadrupoles: solving the heat equation through integral transforms*. Wiley edition